Enhanced Piezoelectricity by Polarization Rotation through Thermal Strain Manipulation in PbZr$_{0.6}$Ti$_{0.4}$O$_3$ Thin Films

Sizhao Huang, Evert Houwman,* Nicolas Gauquelin, Andrey Orekhov, Dmitry Chezganov, Johan Verbeeck, Sixia Hu, Gaokuo Zhong, Gertjan Koster, and Guus Rijnders

Lead based bulk piezoelectric materials, e.g., PbZr$_x$Ti$_{1-x}$O$_3$ (PZT), are widely used in electromechanical applications, sensors, and transducers, for which optimally performing thin films are needed. The results of a multi-domain Landau–Ginzberg-Devonshire model applicable to clamped ferroelectric thin films are used to predict the lattice symmetry and properties of clamped PZT thin films on different substrates. Guided by the thermal strain phase diagrams that are produced by this model, experimentally structural transitions are observed. These can be related to changes of the piezoelectric properties in PZT(x = 0.6) thin films that are grown on CaF$_2$, SrTiO$_3$ (STO) and 70% PbMg$_{1/3}$Nb$_{2/3}$O$_3$-30% PbTiO$_3$ (PMN-PT) substrates by pulsed laser deposition. Through temperature en field dependent in situ X-ray reciprocal space mapping (RSMs) and piezoelectric force microscopy (PFM), the low symmetry monoclinic phase and polarization rotation are observed in the film on STO and can be linked to the measured enhanced properties. The study identifies a monoclinic -rhombohedral M_C-M_A-R crystal symmetry path as the polarization rotation mechanism. The films on CaF$_2$ and PMN-PT remain in the same symmetry phase up to the ferroelectric-paraelectric phase transition, as predicted. These results support the validity of the multi-domain model which provides the possibility to predict the behavior of clamped, piezoelectric PZT thin films, and design films with enhanced properties.

1. Introduction

PbZr$_x$Ti$_{1-x}$O$_3$ (PZT) is one of the most widely used ferroelectric and piezoelectric solid solution materials because of its large room temperature spontaneous polarization and piezoelectric coefficient values. An enhanced piezoelectric response of PZT is found for compositions close to the morphotropic phase boundary (MPB) for x = 0.48.[1] This correlation between structural change and properties has been well explained by thermodynamic models coupled to microstructural analysis. Theoretically, both the polarization rotation mechanism[2–4] and easy domain wall motion[5,6] in PZT near the MPB contribute to the flattening of the free energy landscape. The polarization rotation in the (1-10) plane of the pseudo-cubic unit cells under a (001) oriented field becomes easier by the low energy barrier between the tetragonal (denoted as **T**) and rhombohedral phases (**R**). The discovery of the intermediate, low symmetry, monoclinic C, A and B phases (**M_C**, **M_A**, or **M_B**) near the compositional MPB, suggested the higher order extension of the expression for the free energy in the Landau-Ginzburg-Devonshire (LGD) models,[7–10] and was followed by a series of studies on the polarization rotation path through the free energy landscape. For instance, Fu and Cohen proposed an electric-field induced rhombohedral-monoclinic-tetragonal (**R-M_A-T**) transition path in the MPB PZT alloy,[2] whereas Noheda et al. suggested another complex path, **R-M_A-Orthorhombic**(denoted as **O**)-**M_C-T**.[4] Huang et al. simulated the unexpected Triclinic

S. Huang, E. Houwman, G. Koster, G. Rijnders
MESA+ Institute for Nanotechnology
University of Twente
Enschede 7522 NH, The Netherlands
E-mail: e.p.houwman@utwente.nl

N. Gauquelin, A. Orekhov, D. Chezganov, J. Verbeeck
Electron Microscopy for Materials Science (EMAT)
University of Antwerp
2020 Antwerp, Belgium

S. Hu
Core Research Facilities
Southern University of Science and Technology
Shenzhen 5180551, China

G. Zhong
Shenzhen Key Laboratory of Nanobiomechanics
Shenzhen Institutes of Advanced Technology
Chinese Academy of Sciences
Shenzhen 518055, China

© 2024 The Authors. Advanced Materials Interfaces published by Wiley-VCH GmbH. This is an open access article under the terms of the Creative Commons Attribution License, which permits use, distribution and reproduction in any medium, provided the original work is properly cited.

**ADVANCED
SCIENCE NEWS**

www.advancedsciencenews.com

**ADVANCED
MATERIALS
INTERFACES**
Open Access

www.advmatinterfaces.de

(denoted as **Tri**) and M_C states as a function of compositional modulation, which were also associated with the large electromechanical response of the near-MPB compositions.[11] Also the temperature mediated M_c-M_A-T transitions[12] and the strain induced R-M_A-M_C phase transitions in $BiFeO_3$ thin films[13,14] hinted toward new strategies to design piezoelectric materials (in thin film form) with enhanced functional properties, benefitting from these phase transition paths. For instance, Liu. et al. showed experimentally a five times increase in the effective piezo electrical parameter d_{33} as compared to the bulk phase during the polarization rotation switching in a PZT bilayer film.[15] The strong piezoelectricity of PZT at the MPB in PZT can thus be associated with a transition between different phases via a phase that in X-ray diffraction shows up as a crystallographic monoclinic phase. Theoretical argumentation and experimental evidence strongly suggests that the formation of nanodomains near the MPB can be this (apparent) monoclinic phase.[16–18] Jin et al.[16] initially used this model to describe the phase changes in several PMN-PT compositions, as well as in PZN-PT, assuming the miniaturization of tetragonal domains. These tetragonal, ferroelectric nanodomains can rearrange themselves under influence of external stress or applied field, because of the very low domain wall energies, resulting in what was named an "adaptive phase" with high mechanical stress and electrical field responsivity and thus strong piezoelectricity. Recently there is also much interest in other solid-solution materials with large piezoelectricity, which are often of the relaxor type.[19–22] Noteworthy is the extremely high piezoelectric coefficient d_{33} ranging from 3400 to 4100 pm V^{-1} in 1% Sm-doped PMN-PT single crystals.[23] Sm-doped PMN-PT thin films on a PZT buffer layer on Si were shown to an effective e_{31} value of 20 C m^{-2}, surpassing the best values of PZT and Nb-doped PZT thin films.[24] Liu et al. discovered a different method to achieve a d_{33} value of 1098 pm/V in Na-deficient epitaxial $NaNbO_3$ thin films, in which local heterogeneity arises from the formation of nanopillar regions.[25] Li et al. used $Ba(Zr_{0.1}Ti_{0.9})O_3$ microplatelet templates to fabricate textured, rhombohedral $Pb(Zr_{0.55}Ti_{0.45})O_3$ bulk ceramic material with strongly enhanced $d_{33} = 760$ pm V^{-1}, as compared to the same PZT composition without the use of the template material.[26] These examples show the importance of understanding the origin and workings of the monoclinic phase associated with the large piezoelectricity.

Notwithstanding these advances, a more generally applicable phenomenological model of the structural change and piezoelectric properties of perovskites near the MPB, such as PZT, in clamped thin films remains desirable.[27,28] Khukar, Pertsev et al. analyzed an a/c tetragonal domain structure (denoted here as the two-domain model) on the basis of LGD phenomenological theory to describe the piezoelectric response of bi-axially strained, poly-domain, tetragonal, ferroelectric thin films.[29–31] Houwman et al. argued that an $a/b/c$ domain structure is more appropriate for biaxially strained, tetragonal films and developed what was termed a "three-domain model".[32] Note that both the two and three-domain models also predict and describe the properties of other phases than the tetragonal phase, and phase changes under changing substrate strain and/or temperature. More specifically, in case the domains in the $a/b/c$ domain structure miniaturize into nanodomains, the $a/b/c$ phase of the "three-domain model" can show up in X-

ray diffraction as an apparent monoclinic phase with its associated enhanced piezoelectric properties, according to the adaptive phase model. Other authors discussed adapted similar models to describe the experimental situations in which there is uniaxial, or anisotropic biaxial in-plane strain.[33–35] Vergeer et al. applied successfully the three-domain model to PZT thin films with different compositions under varying thermal expansion mismatch strain of the film with the substrate (S_m^0).[36]

Here we discuss the experimentally determined structural and piezoelectric properties of PZT(x = 0.6) thin films, clamped on different substrates. In bulk this composition has a rhombohedral lattice symmetry, but other symmetries are found or thin films depending on the substrate used. These results are interpreted within the three-domain model. The main results of this model discussed here are i) a structural phase diagram showing crystal symmetry transitions as function of temperature and misfit strain S_m^0; ii) the room temperature, zero-field piezoelectric response (d_{33}) as function of S_m^0; iii) a structural phase diagram as function of applied out-of-plane oriented electrical field and misfit strain.[32] These phase diagrams highlight effects of S_m^0 created during the pulsed laser deposition (PLD) process, which have not been discussed extensively in literature before. Different from the conventional epitaxial misfit strain (S_m), the strain S_m^0 assumes that the bulk of the film is fully relaxed at deposition temperature and the strain builds up during cooling down to room temperature. S_m^0 is therefore the relevant strain parameter for thick films (usually much thicker than the strain relaxation layer with thickness in the range 5–20 nm). A large film thickness is especially relevant for piezoelectric device applications. Only for very thin films S_m^0 is determined by the epitaxial misfit strain.

In this work we validate the three-domain model experimentally using the structural and properties phase diagrams from Ref. [36] as a guide. We selected the PZT (x = 0.6) composition because of its predicted rich structural temperature-strain phase diagram and excellent piezoelectric properties for one of its structural phases. By changing the thermal expansion coefficient (CTE) of the substrate, a tetragonal T phase is obtained at room temperature when the film is grown on CaF_2 substrate (the PZT film is denoted as PZT-C); a monoclinic-c (M_C) phase for growth on $SrTiO_3$ (STO) (denoted as PZT-S) and a R phase for growth on PMN-PT (denoted as PZT-P). The piezoelectric properties of the three PZT films were measured and found to be in reasonable correspondence with the predicted values. These results indicate that substrate induced thermal strain is a critical and useful method to manipulate structure and properties of piezoelectric thin films. Further the crystal structures were investigated as function of applied field. Interestingly, we find indications that in the case of the PZT-S film, which is initially in the M_C phase, a structural change to the M_A phase is observed, which is associated with polarization reorientation.

The results support the validity of the phase diagrams of Ref. [32] and are a strong support for the applicability of the three-domain model, which can therefore be very useful for optimization and design of piezoelectric of clamped poly-domain thin films with outstanding properties.

ADVANCED
SCIENCE NEWS

www.advancedsciencenews.com

ADVANCED
MATERIALS
INTERFACES

www.advmatinterfaces.de

2. Sample

Pulsed laser deposition (PLD) was used to deposit (001)-oriented, 1 μm thick PZT (x = 0.6) films, and a 40 nm SrRuO₃ (SRO) bottom electrode on single crystal substrates of CaF₂(001), STO(001) and PMN-PT(001), respectively. No top electrode is deposited. The films were deposited at 600°C at an oxygen pressure of 0.13 mbar using a pulsed KrF excimer laser with a fluence on the target of 2.5 J cm⁻² at a repetition rate of 4 and 10 Hz for ablation from the polycrystalline SRO and 10% Pb-enriched PZT targets, respectively. The thickness of 1 μm was deliberately chosen to ensure that the bulk of the PZT is subject to substrate induced strain due to thermal expansion mismatch, while only a thin interfacial layer is affected by the epitaxial strain from the substrate. 0.1° miscut STO substrates (CrysTec GmbH) were etched to obtain a single TiO_2 termination with well-defined terrace features. STO has a cubic lattice structure with a lattice constant of 3.905 Å at room temperature, and an almost temperature independent coefficient of thermal expansion (CTE) of 11×10^{-6} K⁻¹.[37] The used rhombohedral PMN70-PT30 substrate material exhibits a paraelectric-ferroelectric phase transition when cooling through the Curie point at 125°C.[38] The PMN-PT substrates (SurfaceNet GmbH) show at room temperature typically surface features of 10–20 nm height differences caused by the polarization domain structure. The CTE is highly temperature dependent and was reported to be $\approx 3.1 \times 10^{-6}$ K⁻¹ at room temperature in the rhombohedral phase (lattice constants $a = 4.019$Å, with $\alpha = 89.91°$ at 25°C),[39] changing to 10.7×10^{-6} K⁻¹ in the cubic phase ($a = 4.020$ Å at ≈ 300 °C).[40] CaF_2 has a cubic lattice structure with lattice parameter $a = 5.45$ Å at room temperature and a constant CTE of 18×10^{-6} K⁻¹ (as determined form our XRD experiments).

The crystalline structure of the films were investigated with X-ray diffraction (XRD) using a Panalytical X'pert MRD lab system. Asymmetrical reciprocal space mappings (RSMs) were obtained using a Panalytical X'pert MRD with an Anton Paar DHS 900 module and a Rigaku Smartlab 9 kW source. Temperature-dependent reciprocal space maps (RSMs) were used to define the lattice strain and symmetry at different temperatures. Atomic force microscopy (AFM) and piezoelectric force microscopy (PFM) measurements were performed with a Bruker Icon atom force microscope using a Cr/Pt conductive coating. A substrate of periodically-poled lithium niobate (PPLN) (from Bruker) was used as a standard PFM sample for calibration of the piezoelectric properties.

The films appeared too leaky to be used with a metallic top electrode, preventing the application of a large external field for polarization hysteresis measurements. Instead we used an ionic gel (IG) that was covered with a Au layer as top electrode,[41] allowing field biasing without inducing electronic leakage. However, the maximum possible applied field was limited. Alternatively we used the calibrated PFM to locally apply a field.

3. Results and Discussion

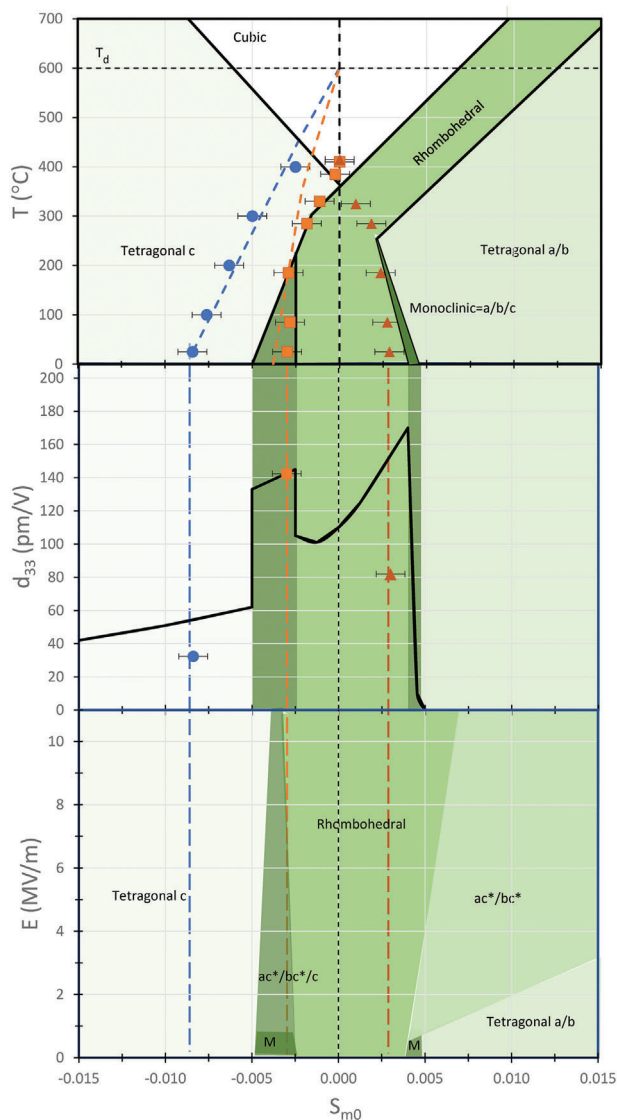### 3.1. Phenomenological Approach and Phase Diagram

In order to be able to interpret our experimental results in terms of the three-domain model, an estimation of the substrate induced in-plane thermal misfit strain as function of tempera-

ture, $S_m^0(T)$ is needed. In the Supplementary Information we discuss the procedure to calculate $S_m^0(T)$, which includes the effects of mismatch in thermal expansion between substrate and clamped film and the unit cell expansion due to the paraelectric-ferroelectric phase transition when cooling down from the deposition temperature through the Curie temperature to room temperature. For this theoretical approach one needs the CTEs of film and substrate and the temperature dependence of the polarization. For the latter we used the approximation $P_s(T) = P_s(RT)\sqrt{1 - T/T_C^*}$ ($P_s(RT)$ is the room temperature saturation polarization and T_C^* the Curie temperature of the clamped film, which might be different from the bulk Curie temperature $T_C = 364$ °C for PZT(0.6)). For the PZT-P film on the PMN-PT substrate, which has a highly non-linear thermal expansion in the temperature range of interest, the calculation of $S_m^0(T)$ appeared to be unreliable and we only use the experimentally derived temperature-strain path.

The mismatch strain can also be determined from the lattice parameters measured as function of temperature. It appears that for the PZT-P film the substrate paraelectric-ferroelectric phase transition plays an important factor in the value of $S_m^0(T)$, whereas for the other films the CTE mismatch is the dominating factor. In Figure S1b (Supporting Information) the calculated and experimentally determined temperature-strain paths are shown. These $S_m^0(T)$ paths are also plotted in the phase diagram of **Figure 1a** (adapted from Ref. [36]). We can make the following observations: i) the $S_m^0(T)$ for PZT-C is compressive at all temperatures and its path shows a single phase transition from the paraelectric cubic phase to the tetragonal **T** phase near 450°C; ii) for the PZT-P film $S_m^0(T)$ is slightly positive, reflecting small tensile strain. The strain path suggests a cubic to rhombohedral phase transition around the bulk Curie temperature; iii) the calculated $S_m^0(T)$ path for PZT-S indicates that this film changes from the paraelectric cubic phase at deposition temperature into a single *c* domain, **T** phase near 400°C upon cooling from the deposition temperature at 600°C. On further cooling, at $\approx$250°C, the film enters the tetragonal *a/b/c* poly-domain phase of the three-domain model, which experimentally shows up as a monoclinic **M** phase. Further details on the model, that is the basis of the phase diagram, can be found in Ref. [36] and the Supplementary Information. In comparison with the compositional phase diagram of bulk PZT, this figure shows that different crystal symmetries can be obtained by tuning the substrate induced strain.

In the second diagram (Figure 1b) the room temperature (zero field) piezoelectric coefficient d_{33}, obtained from the three-domain model for this PZT composition is shown as function of S_m^0. This $d_{33}(S_m^0)$ dependence shows large and stepwise changes of d_{33} in the strain range $S_m^0 = -0.01$ to 0.005, for which reason this PZT-composition was chosen for the present study. Further, it is important to note that this strain range is practically accessible with substrates on which PZT can be grown heteroepitaxially.

The third phase diagram (Figure 1c) shows the room temperature symmetries (phases) of strained PZT(0.6) films under an applied electrical field. For the $S_m^0(RT)$ values the PZT-C and PZT-P films do not show a phase transition under applied fields (up to 200 kV cm⁻¹, here shown up to 110 kV/cm), but the PZT-S film is expected to show a phase transition from the poly-domain a/b/c phase or monoclinic phase to the **R** phase at $E\approx$60–80 kV cm⁻¹.

**ADVANCED
SCIENCE NEWS**

www.advancedsciencenews.com

**ADVANCED
MATERIALS
INTERFACES**
Open Access

www.advmatinterfaces.de

Figure 1. a) Simulated and experimental strain-paths (S_m^0(T)) drawn in the theoretical phase diagram of PZT(x = 0.6), derived from the three-domain model and reused with permission from Refs. [21] and [25]. For compressive thermal misfit strain S_m^0 larger than −0.005, a tetragonal single (out-of-plane oriented) domain c-phase is predicted; The central region for stress around $S_m^0 = 0$ is predicted to have a rhombohedral symmetry, r-phase, and for $S_m^0 > 0.005$ a tetragonal (in-plane) a/b multidomain phase arises. The intermediate regions form a tetragonal $a/b/c$ multidomain phase that shows experimentally up as having a monoclinic symmetry and forms bridges between the rhombohedral and tetragonal phases. At high temperatures above T_c the PZT is in the cubic phase. The dashed blue, orange and purple lines indicate the calculated misfit strains of PZT-C, PZT-S and PZT-P, respectively, when deposited at a temperature of 600 °C. b) Theoretical piezoelectric coefficient d_{33} as function of the room temperature strain. The symbols indicate the experimental d_{33} values of each sample at the specific experimentally determined room temperature strain S_m^0 (RT). The vertical error bar is estimated as <±20, 20 and 10 pm/V for PZT-C, PZT-S and PZT-P, respectively; c) Electric field against thermal strain of PZT(x = 0.6) thin films phase diagram. The dashed lines show PZT thin films symmetry against the electrical field. The $ac*/bc*/c$ phase represents tetragonal a, b and c-domains in which the a and b domains have a small polarization vector component in the out-of-plane c direction caused by the applied field. Idem for the $ac*/bc*$ phase.

3.2. Experimental Results
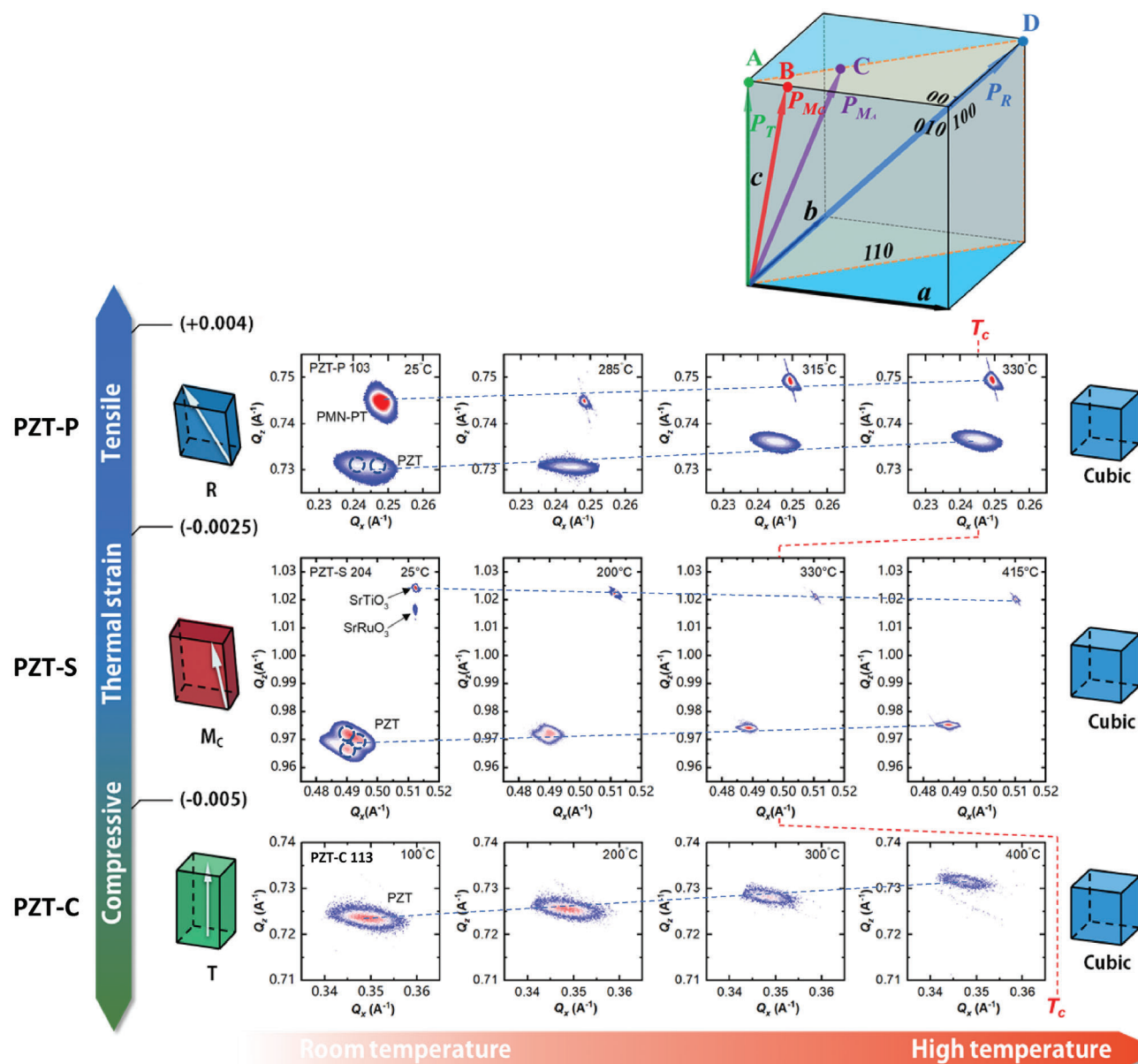
3.2.1. Film Composition

The Zr/Ti ratio of the PLD target was nominally 0.60:0.40. Its stoichiometry was measured by X-ray fluorescence (XRF) to be 0.61:0.39. Considering the stoichiometric transfer of Zr and Ti by PLD one may expect a similar ratio in the deposited films. The composition of the PZT-S film was investigated by He-Rutherford Back Scattering (RBS) and found to be 0.67:0.33 (Figure S12, Supporting Information). RBS accuracy is known to be better than ≈ 5%. The observed difference in target and film composition might suggest a somewhat non-stoichiometric transfer of the B-site elements to the film. We have no reason to assume that the Zr/Ti ratio is different for the PZT-C and PZT-P films. Accurate knowledge of the stoichiometry is important, since the phase diagrams change substantially in the range 0.5:0.5 to 0.7:0.3. Calculations (not presented here) showed that within the three-domain model the $a/b/c$ phase disappears for larger Zr content, whereas the **R** phase disappears for larger Ti content. Only in a narrow range around 0.60:0.40 both the $a/b/c$ and **R** phases are present. This aspect was not investigated further, but may account for some differences between calculated and observed properties.

3.2.2. Structural Analysis – Temperature Dependence

The crystalline quality of the films was investigated by X-ray diffraction $\theta - 2\theta$ scans and reciprocal space mapping (Figures S4 and S5, Supporting Information; **Figure 2**). From the $\theta - 2\theta$ scans we conclude that no other phases are present in either of the three films.

Temperature dependent RSMs were measured (Figure 2). The PZT-C(113) reflections (in pseudocubic lattice notation) correspond to a tetragonal unit cell with the long axis out-of-plane, corresponding to the **T** phase. The c/a lattice parameter ratio decreases with increasing temperature (Figure S1c, Supporting Information). The broad PZT-P(002) peak in the $\theta - 2\theta$ scan of Figure S4 (Supporting Information), as compared to the PZT-S peak, is attributed to the multidomain structure of the underlying PMN-PT substrate. The PZT-P(103) reflections can be interpreted very well in terms of a rhombohedral symmetry. This is also reflected in the ratio $c/a = 1$ at all temperatures (Figure S1c, Supporting Information). At room temperature the four poly-domain peaks, arising from the four possible <111> orientations of the polarization axis in the rhombohedral unit cell, overlap two by two. Therefore only two reflections can be seen. This arrangement of structural domains corresponds to previous calculations of asymmetrical RSMs for **R** symmetry,[42] as well as with other studies. For instance Frano et al. showed that the broad substrate diffraction peak of a LaNiO$_3$ thin film, can be explained by a poly-domain structure with rhombohedral symmetry.[43] The PMN-PT single crystal substrate also has a rhombohedral crystal symmetry at room temperature, which converts into a tetragonal phase at ≈200 °C and becomes cubic at 250 °C.[39,40] In contrast, the PZT-P film still shows visible and separate (rhombohedral) reflections peaks up to 285 °C. Therefore it can be concluded that the rhombohedral phase is due to the PZT-P itself rather than caused by

ADVANCED
SCIENCE NEWS

www.advancedsciencenews.com

ADVANCED
MATERIALS
INTERFACES
Open Access

www.advmatinterfaces.de

Figure 2. Top row left to right: pseudocubic $(103)_{pc}$ RSMs of PZT-P measured at 25, 285, 315, and 330°C, respectively. Two PZT domain peaks (indicated by the dashed circles) are visible at 25 °C. These peaks move closer at 285°C, and have merged in a single domain peak above 315°C. The crystal symmetry shows a crossover from rhombohedral symmetry at low temperature to cubic symmetry at high temperatures. Middle row: $(204)_{pc}$ RSMs of the PZT-S film and the STO substrate at 25, 200, 330, and 415°C. Three PZT domain peaks are visible at 25°C, that move closer at 200°C and merge at 330°C. The RSMs correspond to a M_C to cubic transition. The bottom row shows $(113)_{pc}$ RSMs of PZT-C at 100, 200, 300, and 400 °C, indicating the change from tetragonal to cubic lattice symmetry. The unit cell schematics at the left indicate the polarization directions. The red dashed line indicates the approximate ferroelectric-paraelectric transition temperature (T_C).

imprint of the symmetry phase of the substrate. We expect that this is also true at room temperature. Thus the phase of the PZT-P film is determined by the temperature-dependent, substrate induced strain $S_m^0(T)$ and not by epitaxial strain.

The low temperature (−204) RSMs of the PZT-S sample show three separate reflections, that can be described by M_C, symmetry. Similar reflection structures have been reported in studies on BiFeO₃.[44,45] At temperatures above ≈200 °C the reflections can-

not be separated and the single reflection peak, corresponding to a tetragonal symmetry, or T phase is applicable.

From the RSMs the in-plane and out-of-plane lattice parameters (indicated by respectively a and c) of all PZT films were determined as function of temperature (Figures S1a, S2, and S3, Supporting Information). From these data the strain parameter S_m^0 was determined as function of temperature and these experimentally determined strain-temperature paths are drawn in the
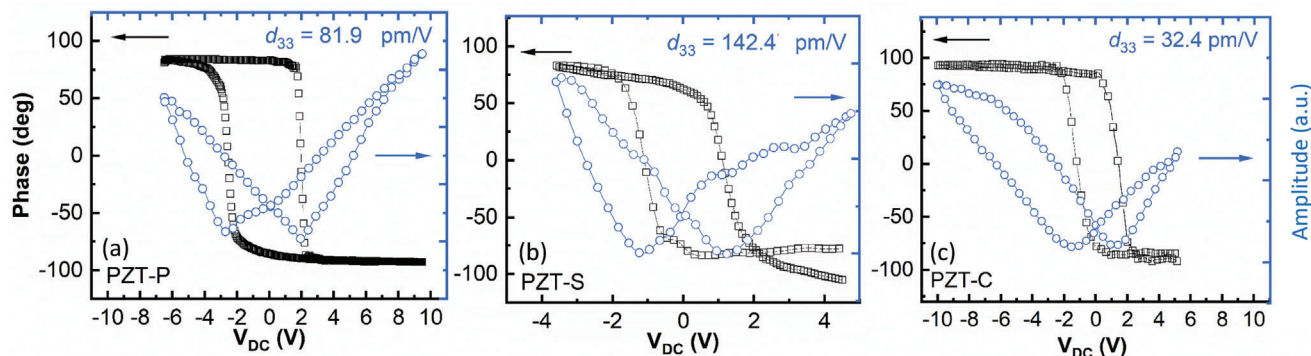
Figure 3. Piezo-force microscopy phase and amplitude loops of a) PZT-P, b) PZT-S, and c) PZT-C. The measured d_{33} value is given in each figure.

phase diagram of Figure 1a. (See Supplementary Information for a detailed discussion of how these lines were obtained.).

3.2.3. Piezoelectric Properties

The PZT-S at room temperature shows the apparent monoclinic symmetry, also found for the bulk PZT(MPB) composition, for which strongly enhanced piezoelectricity is found. Therefore we investigated also the piezoelectric properties of these films as the three-domain model predicts a significant enhancement of the piezoelectric parameter d_{33} in the $a/b/c$ phase, as can be seen from Figure 1b.
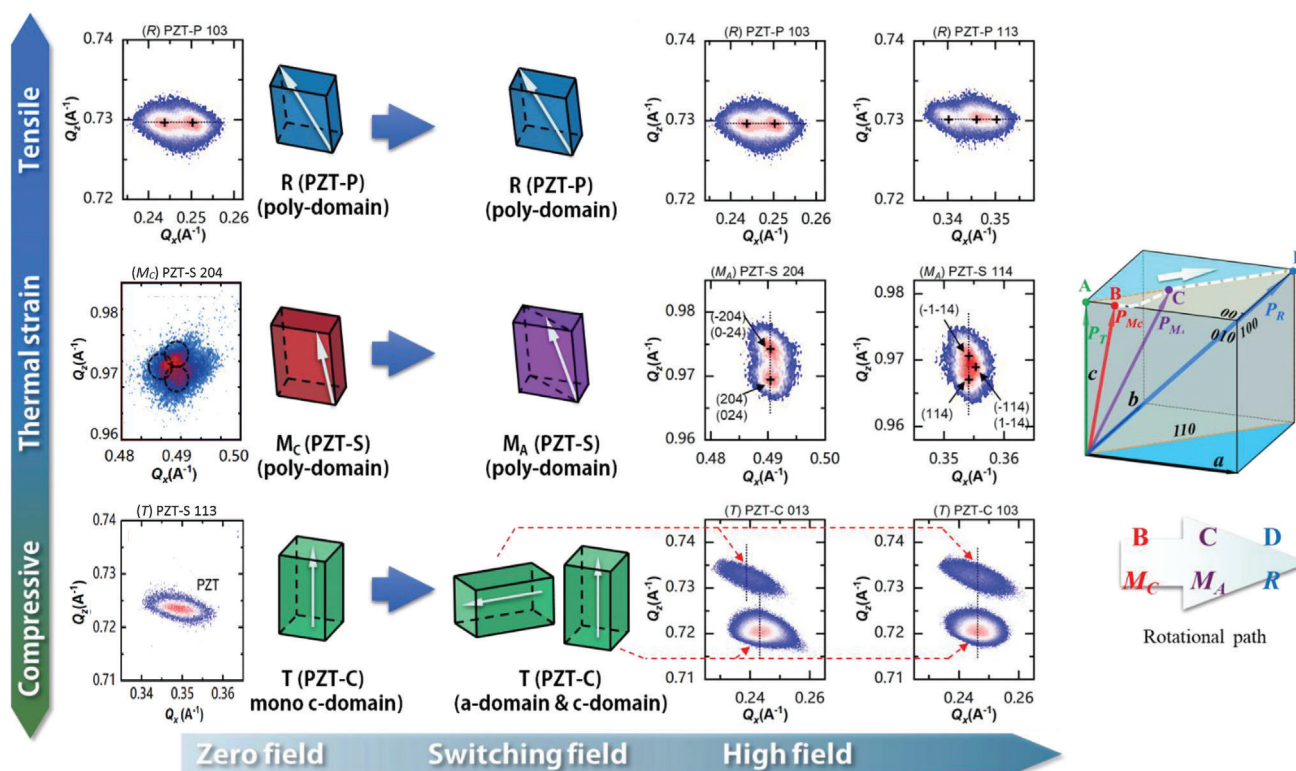
Piezo force microscopy was used to investigate the ferroelectric domain structure and to determine the piezoelectric coefficients. In Figure S7 (Supporting Information) it is shown that all three films can be switched. The PZT-P and PZT-S films show a polydomain structure in the unpolarized state with domain dimensions of the order of hundred nanometers. The PZT-C film is uniformly poled upward in the pristine state, suggesting a significant build-in field, which is attributed to a strain gradient at the substrate/film interface.[46] **Figure 3** shows the calibrated polarization hysteresis loops measured by PFM at room temperature. The obtained zero-field d_{33} values are plotted in Figure 1b. It is seen that the value measured for PZT-S is accurately predicted by the model. The experimental values for PZT-P and PZT-C are significantly less than the value for PZT-S, as is also predicted by the model. The discrepancy in calculated and measured values for the PZT-P and PZT-C films might be due to an overestimation of d_{33} by the three-domain model for the c- and r-phases, which are based on single domain properties, whereas a real film consist of multiple grains and ferroelectric domains. Due to strain developing at grain boundaries and at the domain wall between different r-domains it is expected that the piezoelectric response is reduced. A second reason for the discrepancy could be the limited displacement resolution of the PFM measurement, which is estimated to be less than 20, 20 and 10 pm/V for the PZT-C, PZT-S and PZT-P samples respectively. However, as the value for the PZT-S film is accurately predicted it appears that the PFM measurement method is reliable and the explanation by the inadequacy of the three-domain model to include the multi-domain character of the c- and r-phases seems more applicable.

3.2.4. Symmetry under Applied Field

Further we studied the change of the crystal symmetry of the differently strained films under applied field (in the out-of-plane direction) and interpret the results in terms of the field-strain phase diagram of Figure 1c. Previous studies on PZT single crystals suggest that polarization rotation can be induced by small field strengths and involve a monoclinic phase.[47] Here, we applied an ionic gel to the leaky thin films in order to be able to apply an electric field over a large film area, allowing for in situ XRD measurements.[41,48] The voltage that could be applied to the IG top electrode was 1 V. The RSMs at 0 V and 1 V voltage bias for the different films are shown in **Figure 4**.

From the RSMs in the first row it is seen that the zero field rhombohedral symmetry of the (PZT-P) film is maintained at non-zero field. PFM imaging on bare films show that the film can be poled and switched, using tip voltages of +/−7 Volt (Figure S7, Supporting Information). From the combination of PFM measurements and RSM mapping at high field, it is concluded that the PZT-P remains in the **R** phase at finite fields in accordance with the model prediction, shown in Figure 1c.

From the RSMs of the PZT-S it is inferred that the crystalline symmetry changes from M_C to M_A symmetry, when the applied voltage is changed. This corresponds to a change of the polarization rotation plane from the pseudocubic (100) to the (110) plane. This suggests that upon further increase of the field the polarization might rotate further toward the [111] direction (in the (110) plane), corresponding to rhombohedral symmetry. The M_C-M_A-R polarization rotation path corresponds to the predicted symmetry changes in the electric field- misfit strain phase diagram in Figure 1c. The region in the phase diagram labelled with $ac*/bc*/c$, (in the three-domain model this means that the a and b domains in the $a/b/c$ structure have polarization vectors that are slightly rotated in the out-of-plane direction, this is the $c*$ component) shows apparently in XRD measurements up as a phase with M_A symmetry, whereas the $a/b/c$ region shows experimentally a M_C symmetry. Thus we have some experimental evidence for the M_C-M_A section of a possible M_C-M_A-R path in a clamped PZT(0.6) thin film, induced by an out-of-plane applied electrical field, similar to polarization rotation paths suggested to be present in unstrained PZT(MPB), as mentioned in the introduction. To our knowledge such a symmetry path way has not been reported before for a non-MPB PZT composition,

ADVANCED
SCIENCE NEWS

www.advancedsciencenews.com

ADVANCED
MATERIALS
INTERFACES
Open Access

www.advmatinterfaces.de

Figure 4. From left to right: RSMs of differently strained (indicated by lefthand arrow) PZT thin films measured in zero applied field (left column) and using an electrostatic gating voltage on the top electrode (right two columns). For PZT-P no change in the symmetry of the lattice could be discerned, it remains rhombohedral for the field applied. For PZT-S the change in RSMs indicate a change from monoclinic-C (M_C) to monoclinic-A (M_A) symmetry, which has a more rhombohedral character. This corresponds to a rotation of the polarization vector from out-of-plane to the body-diagonal of the pseudocubic unit cell. The PZT-C sample shows at finite bias field the appearance of in-plane oriented tetragonal domains, indicating ferroelastic switching during the poling, and implying also that the tetragonal symmetry remains after 180° switching. The M_C to M_A phase transition of PZT-S implies a different polarization switching mechanism, namely through polarization rotation, than for the PZT-P (lattice and thus polarization extension) and PZT-C (lattice and thus polarization extension and 90° domain switching).

nor for a clamped thin film configuration as opposed to a single crystal.

Naively one would expect in the PZT-C film only unit cell extension in the out-of-plane direction under an applied field, which is severely hampered by the clamping to the substrate. However, in the poling experiment with the IG top electrode also a fraction of in-plane oriented tetragonal domains appear under applied field, which surprisingly are oriented only in one direction (as can be deduced from the (103) and (013) RSMs). In our previous work[48] it was suggested that the appearance of only *a*-domains in this sample probably is due to a preferential step edge direction on the surface of the substrate due to a miscut of the substrate.[49,50] Figure S13 (Supporting Information) shows SRO pseudocubic (113) RSMs in four orthogonal principal in-plane directions of the CaF$_2$ substrate. These indicate a slight uniaxial tilting of the SRO bottom electrode layer, which may account for the anisotropic formation of in-plane tetragonal domains. In addition, the unexpected partial switching from *c* to *a* domains might arise from the incomplete screening at the top ferroelectric-gel interface, causing the need of *a*-type closure domains.[51]

Overall, we conclude that changing symmetries in the PZT films on different substrates under influence of an applied field support the validity of the phase diagram arising from the three-domain model.

4. Discussion

From the above it is concluded that the experimentally determined structural phases at different temperatures are predicted by the three-domain model: tetragonal symmetry of the PZT-C film with negative $S_m^0(T)$, causing compressive, in-plane thermal strain up to the ferroelectric-paraelectric phase transition temperature at ≈450 °C; rhombohedral symmetry of the PZT-P film with $S_m^0(T) \approx 0$ and what shows up as monoclinic M_C symmetry in PZT-S for small compressive strain at lower temperatures, transiting to tetragonal symmetry above ≈250 °C, and ending in the cubic, paraelectric phase above about the bulk Curie temperature of this PZT-composition. Thus by using different substrates that create different in-plane strains, the PZT(x = 0.6) films show structural transitions between the *T*, M_C, and *R* phases when the substrate-induced strain changes from compressive to tensile. Also, the Curie temperatures of the strained films are well described by the three-domain model predictions in the first phase diagram.

2400048 (7 of 9)

Thus next to the commonly discussed Morphotropic Phase Boundary (which has been identified as a monoclinic phase) between the rhombohedral and the tetragonal compositional phases, we here show that a similar intermediate structural phase arises when the in-plane strain in a clamped PZT(0.6) film is changed from highly compressive to slightly tensile. Some models in literature predict such an intermediate phase, while others miss it. We think that is because LGD based models are often based on the comparison of the free energies of different domain configurations for given strain and temperature and naturally choose the phase with minimum energy as the phase present. Therefore it depends on the different domain configurations included in the comparison, which lowest energy phase is obtained. In the three-domain model used here, the tetragonal $a/b/c$ phase is a very special phase, that allows a domain structure with zero strain energy and therefore always has the lowest energy if it can be present. Further, the easy change between different domain types in the $a/b/c$ phase causes a significantly larger piezoelectric response than in the phases in which domain switching is hampered by the film clamping. The $a/b/c$ phase is clearly present in the XRD analysis of PZT films with tetragonal bulk properties. However, the properties of PZT films with MPB composition and, as is shown here, even with bulk rhombohedral composition can be well described by the $a/b/c$ domain structure, which structurally show up as a monoclinic phase. This identification can be explained by assuming that the tetragonal $a/b/c$ domains are nanometer sized and what is measured in XRD is the average domain size (see Supplementary Information).

In our experiments three different phases are observed in the room temperature strain regime $S_m^0 = -0.0085....0.0025$. Experimentally it appears to be very difficult to achieve larger (absolute strain values) because of the lack of substrates with suitable CTEs. Note that a CTE = 18 ppm/K of CaF_2 is already very high, whereas large tensile strain in our experience results in cracking of the film, as a mechanism to relax the strain, rather than a large in-plane tensile strain. We note our effort to access the narrow strain regime around $S_m^0 = 0.0045$ with the $a/b/c$ phase between the r-phase and the tetragonal a/b (with only in-plane oriented domains), where a very abrupt and large transition in the piezoelectric response is expected, by bending thin Si wafers with epitaxial STO buffer layers. However, under the required applied bending stress the films cracked and this effort failed.

5. Conclusion

In conclusion, we have studied the effects of thermal misfit strain arising from the use of different CTE single crystal (001) oriented substrates (CaF_2, STO, PMN-PT) on the crystalline and piezoelectric properties of 1 μm PZT(x = 0.6) epitaxial thin films made by pulsed laser deposition. The crystalline symmetries observed in the RSMs of these three samples are different from the symmetry found for the bulk, unstrained material in the cases of larger strain, and these symmetries change with temperature. The observations give a clear picture of the role of thermal misfit strain in these films. The symmetries can be explained in terms of the earlier developed three-domain model for clamped, thick films. Secondly, the piezoelectric properties show an enhancement in the sample on STO with monoclinic symmetry and the change of symmetry with applied field indicates that the polarization ro-

tation mechanism is responsible for the strongly enhanced piezoelectric response as compared to the films on CaF_2 and PMN-PT. Comparison with the model suggest the presence of a M_C-M_A-R rotational path in the PZT film on the STO substrate. This would be the first time such a path is shown experimentally to be present. This finding supports the rotational path mechanism as was originally proposed by Fu and Cohen and provides experimental support for the understanding of the relationship between structures and properties in thin films which show a morphotropic phase boundary

Furthermore, these experimental results are in agreement with the Figure 1 phase diagrams that are predicted by the three-domain model, e.g., the anisotropic in-plane strain induces single in-plane axis ferroelastic switching in PZT-C. The implementation of this model on strained thin films gives us the ability to predict clamped thin film behaviour, and as demonstrated here, allows us to further design films with enhanced properties which is potentially attractive for thin film oxide applications.

Supporting Information

Supporting Information is available from the Wiley Online Library or from the author.

Acknowledgements

Conflict of Interest

The authors declare no conflict of interest.

Data Availability Statement

The data that support the findings of this study are available from the corresponding author upon reasonable request.

Keywords

[1] B. Jaffe, W. Cook, H. Jaffe, *Piezoelectric Ceramics*, Academic Press, London, **1971**.

[2] H. Fu, R. E. Cohen, *Nature* **2000**, *403*, 281.

[3] B. Noheda, Z. Zhong, D. E. Cox, G. Shirane, S.-E. Park, P. Rehrig, *Phys. Rev. B* **2002**, *65*, 224101.

[4] B. Noheda, D. E. Cox, G. Shirane, S.-E. Park, L. E. Cross, Z. Zhong, *Phys. Rev. Lett.* **2001**, *86*, 3891.

[5] F. Xu, S. Trolier-McKinstry, W. Ren, B. Xu, *J. Appl. Phys.* **2001**, *89*, 1336.

[6] Y.-H. Shin, I. Grinberg, I.-W. Chen, A. M. Rappe, *Nature* **2007**, *449*, 881.

[7] B. Noheda, D. E. Cox, G. Shirane, J. A. Gonzalo, L. E. Cross, S.-E. Park, *Appl. Phys. Lett.* **1999**, *74*, 2059.

[8] N. Zhang, H. Yokota, A. M. Glazer, Z. Ren, D. A. Keen, D. S. Keeble, P. A. Thomas, Z.-G. Ye, *Nat. Commun.* **2014**, *5*, 5231.

[9] D. Vanderbilt, M. H. Cohen, *Phys. Rev. B* **2001**, *63*, 094108.

[10] L. Fan, L. Zhang, H. Liu, *Inorg. Chem.* **2021**, *60*, 15190.

[11] N. Huang, Z. Liu, Z. Wu, J. Wu, W. Duan, B.-L. Gu, X.-W. Zhan, *Phys. Rev. Lett.* **2003**, *91*, 067602.

[12] C. Beekman, W. Siemons, T. Z. Ward, M. Chi, J. Howe, M. D. Biegalski, N. Balke, P. Maksymovych, A. K. Farrar, J. B. Romero, P. Gao, X. Q. Pan, D. A. Tenne, H. M. Christen, *Adv. Mater.* **2013**, *25*, 5561.

[13] Z. Chen, Z. Luo, C. Huang, Y. Qi, P. Yang, L. You, C. Hu, T. Wu, J. Wang, C. Gao, T. Sritharan, L. Chen, *Adv. Funct. Mater.* **2011**, *21*, 133.

[14] H. W. Jang, S. H. Baek, D. Ortiz, C. M. Folkman, R. R. Das, Y. H. Chu, P. Shafer, J. X. Zhang, S. Choudhury, V. Vaithyanathan, Y. B. Chen, D. A. Felker, M. D. Biegalski, M. S. Rzchowski, X. Q. Pan, D. G. Schlom, L. Q. Chen, R. Ramesh, C. B. Eom, *Phys. Rev. Lett.* **2008**, *101*, 107602.

[15] G. Liu, Q.i Zhang, H.-H. Huang, P. Munroe, V. Nagarajan, H. Simons, Z. Hong, L.-Q. Chen, *Adv. Mater. Interfaces* **2016**, *3*, 1600444.

[16] Y. M. Jin, Y. U. Wang, A. G. Khachaturyan, J. F. Li, D. Viehland, *J. Appl. Phys.* **2003**, *94*, 3629.

[17] G. A. Rossetti, A. G. Khachaturyan, G. Akcay, Y. Ni, *J. Appl. Phys.* **2008**, *103*, 114113.

[18] A. G. Khachaturyan, *Philos. Mag.* **2010**, *90*, 37.

[19] J. Wang, S. Wang, X. Li, L. Li, Z. Liu, J. Zhang, Y. Wang, *J. Adv. Ceram.* **2023**, *12*, 792.

[20] L. Yang, H. Huang, Z. Xi, L. Zheng, S. Xu, G. Tian, Y. Zhai, F. Guo, L. Kong, Y. Wang, W. Lü, L. Yuan, M. Zhao, H. Zheng, G. Liu, *Nat. Commun.* **2022**, *13*, 2444.

[21] Y. Yan, L. D. Geng, L.-F. Zhu, H. Leng, X. Li, H. Liu, D. Lin, K. Wang, Y. U. Wang, S. Priya, *Adv. Sci.* **2022**, *9*, 2105715.

[22] J. Fu, Z. Yu, A. Xie, Z. Yu, Z. Fu, X. Jiang, T. Li, R. Zuo, *Acta Mater.* **2023**, *254*, 118991.

[23] F. Li, M. J. Cabral, B. Xu, Z. Cheng, E. C. Dickey, J. M. LeBeau, J. Wang, J. Luo, S. Taylor, W. Hackenberger, L. Bellaiche, Z. Xu, L.-Q. Chen, T. R. Shrout, S. Zhang, *Science* **2019**, *364*, 264.

[24] X. Qi, S. Yoshida, S. Tanaka, *IEEE Trans. Ultrason. Ferroelectr. Freq. Control* **2022**, *69*, 1821.

[25] H. Liu, H. Wu, K. P. Ong, T. Yang, P. Yang, P. K. Das, X. Chi, Y. Zhang, C. Diao, W. K. A. Wong, E. P. Chew, Y. F. Chen, C. K. I. Tan, A. Rusydi, M. B. H. Breese, D. J. Singh, L.-Q. Chen, S. J. Pennycook, K. Yao, *Science* **2020**, *369*, 292.

[26] J. Li, W. Qu, J. Daniels, H. Wu, L. Liu, J. Wu, M. Wang, S. Checchia, S. Yang, H. Lei, R. Lv, Y. Zhang, D. Wang, X. Li, X. Ding, J. Sun, Z. Xu, Y. Chang, S. Zhang, F. Li, *Science* **2023**, *380*, 87.

[27] M. Haun, E. Furman, S. J. Jang, L. E. Cross, *Ferroelectrics* **1989**, *99*, 13.

[28] M. J. Haun, Z. Q. Zhuang, E. Furman, S.-J. Jang, L. E. Cross, *J. Am. Ceram. Soc.* **1989**, *72*, 1140.

[29] A. Bartasyte, B. Dkhil, J. Kreisel, J. Chevreul, O. Chaix-Pluchery, L. Rapenne-Homand, C. Jimenez, A. Abrutis, F. Weiss, *Appl. Phys. Lett.* **2008**, *93*, 242907.

[30] V. Koukhar, N. Pertsev, R. Waser, *Phys. Rev. B* **2001**, *64*, 214103.

[31] V. G. Kukhar, N. A. Pertsev, H. Kohlstedt, R. Waser, *Phys. Rev. B* **2006**, *73*, 214103.

[32] a) E. P. Houwman, G. Vergeer, G. Koster, G. Rijnders, Modelling functional properties of ferroelectric oxide thin films with a three-domain structure. arXiv preprint arXiv:1901.10883, **2019**; b) E. P. Houwman, K. Vergeer, G. Koster, G. Rijnders, Functional Properties of Polydomain Ferroelectric Oxide Thin Films, in Correlated Functional Oxides, Eds. N. Nishikawa et al. (eds.), Springer **2017**.

[33] G. Yuan, H. Huang, C. Li, D. Liu, Z. Cheng, D. Wu, *Adv. Electron. Mater.* **2020**, *6*, 2000300.

[34] X. Wan, E. P. Houwman, R. Steenwelle, R. van Schaijk, M. D. Nguyen, M. Dekkers, G. Rijnders, *Appl. Phys. Lett.* **2014**, *104*, 092902.

[35] A. I. Khan, X. Marti, C. Serrao, R. Ramesh, S. Salahuddi, *Nano Lett.* **2015**, *15*, 2229.

[36] K. Vergeer, Structure and Functional Properties of Epitaxial PbZrxTi1-xO3films, PhD-thesis University of Twente, The Netherlands, **2017**.

[37] D. de Ligny, P. Richet, *Phys. Rev. B* **1996**, *53*, 3013.

[38] H. Arndt, G. Schmidt, *Ferroelectrics* **1988**, *79*, 149.

[39] R. Wongmaneerung, R. Guob, A. Bhallab, R. Yimniruna, S. Ananta, *J. Alloys Compd.* **2008**, *461*, 565.

[40] F. Bai, N. Wang, J. Li, D. Viehland, P. M. Gehring, G. Xu, G. Shirane, *J. Appl. Phys.* **2004**, *96*, 1620.

[41] S. Huang, Symmetry and Functional Properties of Clamped Pb(Zr0.6Ti0.4)O3 Tuned by Thermal Strain and Electrostatics Effects, PhD-thesis University of Twente, The Netherlands, **2021**

[42] D. L. Corker, A. M. Glazer, R. W. Whatmore, A. Stallard, F. Fauth, *J. Phys.: Condens. Matter* **1998**, *10*, 6251.

[43] A. Frano, E. Benckiser, Y. Lu, M. Wu, M. Castro-Colin, M. Reehuis, A. V. Bori, E. Detemple, W. Sigle, P. van Aken, G. Cristiani, G. Logvenov, H.-U. Habermeier, B. Pochner, B. Keimer, V. Hinkov, *Adv. Mater.* **2014**, *26*, 258.

[44] Z. Chen, Z. Luo, Y. Qi, P. Yang, S. Wu, C. Huang, T. Wu, J. Wang, C. Gao, T. Sritharan, L. Chen, *Appl. Phys. Lett.* **2010**, *97*, 242903.

[45] K. Saito, A. Ulyanenkov, V. Grossmann, H. Ress, L. Bruegemann, H. Ohta, T. Kurosawa, S. Ueki, H. Funakubo, *Jpn. J. Appl. Phys.* **2006**, *45*, 7311.

[46] M. Boota, E. P. Houwman, M. Dekkers, M. Nguyen, G. Rijnders, *Appl. Phys. Lett.* **2014**, *104*, 182909.

[47] L. Bellaiche, A. García, D. Vanderbilt, *Phys. Rev. B* **2001**, *64*, 060103.

[48] S. Huang, F. Blom, H. Gojzewski, G. Rijnders, G. Koster, *Appl. Phys. Lett.* **2021**, *119*, 262904.

[49] W. Wang, L. Li, J. Liu, B. Chen, Y. Ji, J. Wang, G. Cheng, Y. Lu, G. Rijnders, G. Koster, W. Wu, Z. Liao, *Quantum Mater.* **2020**, *5*, 1.

[50] G. Koster, L. Klein, W. Siemons, G. Rijnders, J. S. Dodge, C.-B. Eom, D. H. A. Blank, M. R. Beasley, *Rev. Modern Phys.* **2012**, *84*, 253.

[51] We note that in ref. [48] it was shown that once the a-domains are created they remain present throughout the whole field cycle, thus contrary to the previous suggestion that the a-domains might be needed for making polarization reversal possible, we think this idea is not supported by the experimental data given in [48].